Available online at www.sciencedirect.com

ScienceDirect

Mendeleev Commun., 2018, **28**, 170–172

Mendeleev Communications

DFT modeling of the first step of plastoquinol oxidation by the iron–sulfur protein of the cytochrome b_6f complex

Leila Yu. Ustynyuk,*[a] Boris V. Trubitsin[b] and Alexander N. Tikhonov[b]

[a] *Department of Chemistry, M. V. Lomonosov Moscow State University, 119991 Moscow, Russian Federation. Fax: +7 495 932 8846; e-mail: leila_ust@mail.ru*

[b] *Department of Physics, M. V. Lomonosov Moscow State University, 119991 Moscow, Russian Federation*

DOI: 10.1016/j.mencom.2018.03.020

DFT analysis of several models for 2,3,5-trimethylbenzoquinol oxidation in the catalytic center of the cytochrome b_6f complex, consisting of the $[Fe_2S_2]$ cluster and its surroundings, has been performed. The comparison of optimized structures with different numbers (14–20) of fixed internal coordinates allowed us to find an optimal model close to the crystal structure.

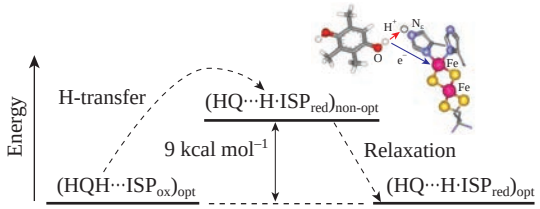

The cytochrome (Cyt) b_6f complex (plastoquinol : plastocyanin oxidoreductase) stands at the crossroad of photosynthetic electron transport pathways.[1–3] In plants and cyanobacteria, there are two photosystems, PSI and PSII, interconnected *via* the membrane-bound Cyt b_6f complex (which includes Cyt *f*, two hemes of Cyt b_6, and $[Fe_2S_2]$ cluster) and mobile electron carriers, plastoquinone (PQ), plastocyanin (Pc): PSII → PQH_2 → b_6f → Pc → PSI (Scheme 1). The crystal structures of the Cyt b_6f complexes from *C. reinhardtii* (PDB entry 1Q90)[4] and *M. laminosus* (PDB entry 1VF5)[5] have been first obtained at a resolution of 3.0–3.1 Å, in the presence of the quinone analogue inhibitor, tridecylstigmatellin (TDS). Oxidation of plastoquinol (PQH_2, the reduced form of PQ) is the rate-limiting step in the chain of electron transfer from PSII to PSI.[2,3] The two-electron oxidation of PQH_2 is provided by two reaction centers, the iron–sulfur cluster $[Fe_2S_2]$ and the low-potential heme b_6^L (see Scheme 1 and Figure 1). There are good reasons to believe that electron transfer from PQH_2 to the iron–sulfur protein (ISP) represents the rate-limiting step of PQH_2 turnover.[3] In the catalytic o-site, PQH_2 is connected (*via* the hydrogen bond) to the N_ε atom of the histidine residue liganding one of two Fe atoms of the ISP (Figure 1). This atom is considered as the recipient of the H^+ ion donated by PQH_2.[1,6]

Earlier attempts of DFT modeling of quinol oxidation by the Cyt complexes of *bc* type were reported.[7–9] Quantum chemical simulation of electron transport in proteins faces with a problem of an adequate choice of the model system picked out from the crystal structure of the protein. To mimic adequately the properties of the enzyme, a model system (the catalytic center + substrates) must be sufficiently large; however, a size of the system may be limited by computer capacities. Another problem is that geometry optimization may cause too strong distortions of the system geometry, being a potential source of confusions. Therefore, the construction of a model system with the architecture close to that in the crystal structure of the Cyt b_6f complex was our first task. Using the program Molsoft ICM-Browser v3.8.5[10] for RMSD calculations, we evaluated the conformity of optimized model systems to X-ray structures (Table 1). The model system consisting of 130 atoms (among them, 71 heavy atoms, including two Fe and four S atoms) is based on the PDB data (code 1Q90).[4] It includes an iron–sulfur cluster $[Fe_2S_2]$ and surrounding amino acid residues (Cys134–Thr135–His136–Leu137–Gly138–Cys139, Cys152, Cys154–His155–Gly156–Ser157). As a model of PQH_2 (fully reduced form of PQ), we used 2,3,5-trimethylbenzoquinol ($TMBQH_2$).[8] Taking into account that in oxidized ISP, His155 is deprotonated and His136 is protonated,[6] we conclude that the total charge of the system equals to $Z = -1$. Since the $[Fe_2S_2]$ cluster of the oxidized ISP represents the diamagnetic species,[11] the multiplicity of the system $m = 1$ (spin $S = 0$, if other is not specified). Calculations were carried out using the program PRIRODA,[12] the functional PBE,[13] and TZ2P Gaussian-type basis sets (for details, see Online Supplementary Materials). Unrestricted Kohn–Sham method was used for all calculations.

Figure 2 depicts the non-optimized structure of the initial system (M0) described above. To avoid unreasonably strong distortions of the system architecture upon the geometry optimiza-

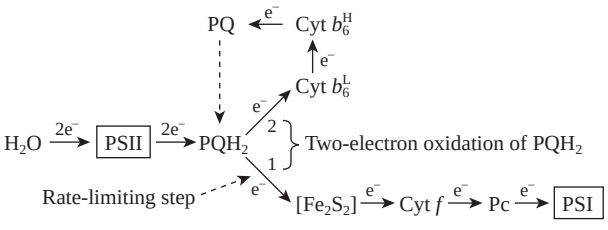

Scheme 1 The Cyt b_6f complex in the chain of electron transport from PSII to PSI.

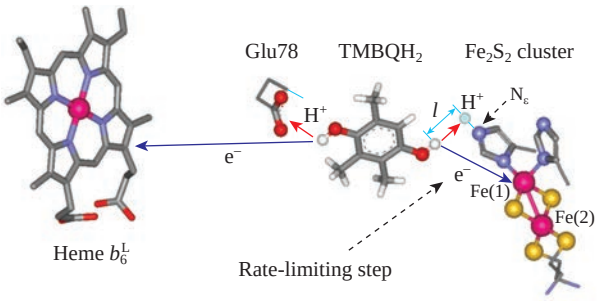

Figure 1 The bifurcation mechanism of two-electron oxidation of quinol.

Table 1 The energy and geometry parameters of models M*i* and products P*i*^{opt} and P*i*^{nop} (*i* = 1–6).

Model	Number of fixed parameters				RMSD/Å	ΔE/kcal mol^{-1}				l_{H-N_ε}/Å		Δl^c/Å
	Total	Distances	Bond angles	Torsion angles		ΔE^M	ΔE_{opt}	ΔE_{nop}	ΔE_{rel}	M	P^{opt}, P^{nop}	
M1	0	0	0	0	–[a]	0	–[b]	–	–	1.643	–	–
M2	14	4	8	2	–[a]	27.6	3.6	17.4[d] 16.6[d]	13.8[d] 13.0[d]	2.068	1.056	1.117[d] 1.095[d]
M3	16	4	8	4	0.99	31.3	0.2	19.9 18.8	19.7 18.6	2.139	1.049	1.463 1.403
M4	18	6	8	4	0.44	31.8	0.5	9.9 10.7	9.4 10.2	2.062	1.051	1.048 1.056
M5	20	8	8	4	0.47	33.5	–0.2	7.8 8.2 *7.7*[e]	8.0 8.4 *8.0*[e]	2.046	1.051 *1.062*[e]	1.034 1.036 *1.023*[e]
M6	14	7	5	2	0.70	27.6	0.1	8.9 9.2	8.8 9.1	2.070	1.050	1.057 1.055

[a] Not determined due to critical changes in geometry of M1 and M2 with respect to the initial structure M0. [b] The energy minimum corresponding to P1^{opt} was not found. [c] The distance between the H atom positions before and after the H-transfer (Figure 1). [d] The structures of non-optimized products (P^{nop}) were obtained using two different approaches as described in the text. The data for the best approximation of two are underlined. [e] The refined values were obtained by detailed scanning of E(P^{nop}) *vs.* the H atom position with regard to His155.[14]

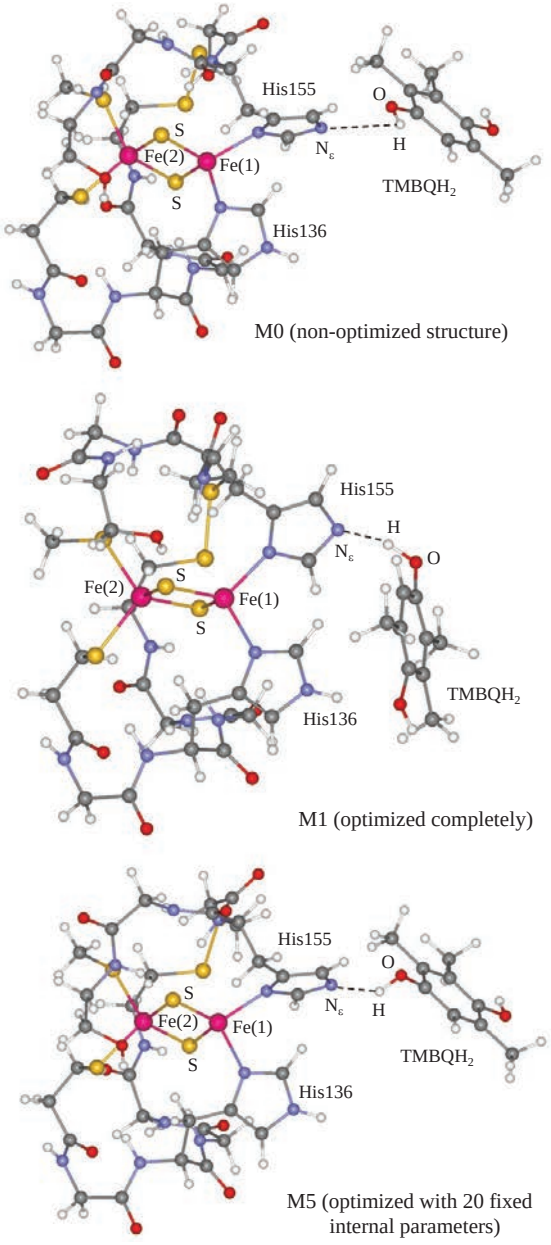

Figure 2 The initial model system M0 (based on the crystal structure data[4]) and optimized systems M5 (Z = –1, m = 1, not distorted) and M1 (strongly distorted with respect to M0).

tion, its structure was constrained by fixing some of internal coordinates. A number of fixed parameters (n) varied in the range from n = 14 to n = 20. The energy and geometry characteristics of optimized systems (models M1–M6) are presented in Table 1. Selecting a set of fixed internal coordinates, we followed the notion that in optimized constrained systems the quinol molecule and the ring of the His155 residue should remain in the close positional relationship as in the initial (non-optimized) system M0, which is the fragment of the crystal structure. In particular, in all the models (with the exception of M1) the distance between the proximal atom O of $TMBQH_2$ and the N_ε atom of His155 was fixed as 2.852 Å. In the model system M1, internal coordinates were not fixed. In the line of structures M2–M5, a number of fixed parameters was increased from n = 14 (M2) to n = 20 (M5). Then we released a number of fixed parameters under the stipulation that the structure of the system was not distorted dramatically. The model M6 was produced by releasing six of twenty fixed parameters in M5, while other parameters (n = 14), that had the most significant impact on the results of optimization, remained fixed. Atomic coordinates in the systems M0–M6 and the list of the fixed internal coordinates for these systems are given in Online Supplementary Materials.

The completely optimized structure M1 (without fixed parameters) and optimized structure M2 (constrained, n = 14) are notably distorted as compared to the initial (non-optimized) structure M0. The quinol position in M1 changes markedly as the result of geometry optimization (Figure 2). In optimized structures M3–M6, the quinol position is similar to that in M0. For formal quantification of the geometry distortion, we compared the RMSD values for optimized structures M3–M6 with respect to the initial structure M0. As one can see from Table 1, the lowest RMSD values were found for the structures M4 and M5 with the maximal numbers of fixed internal coordinates. The total energies ΔE^M of the optimized model systems M2–M6 with respect to the energy of M1 are given in Table 1. Maximal energy was obtained for M5 (Figure 2). Although there is no strict linear relationship between the ΔE^M and RMSD values, rather small RMSD values for M4 and M5 indicate that their architectures are closely related to the crystal structure. Taking together, we conclude that the systems M4 (n = 18) and M5 (n = 20) may be considered as the appropriate structures for modeling $TMBQH_2$ oxidation.

For M4, we also performed geometry optimization of the systems with higher multiplicities (m = 3, 5, 7, 9, and 11). Their energies calculated with respect to the energy of the singlet state of M4 increased with the rise of m and equal to 2.8, 9.8, 9.9,

15.2, and 20.4 kcal mol^{-1} for m = 3, 5, 7, 9, and 11, respectively. The similar result was obtained for M5.[14] This result is in good agreement with the well-established fact that the ground state of oxidized ISP is the singlet state (m = 1, spin S = 0).[11]

Our second task was associated with simulation of the first step of quinol oxidation in the redox center of the ISP. We have calculated the energy effects of the H atom transfer from the OH group of $TMBQH_2$ towards the N_ε atom of His155 (Figures 1 and 2) in the systems M2–M6. As the result of the H-transfer, the hydrogen bond between the OH group and the N_ε atom of His155 ($l_{H–N_\varepsilon} \approx 2$ Å) decreases, forming the covalent bond between the N_ε and H atoms ($l_{H–N_\varepsilon}$ = 1.05 Å). The analysis of the redistribution of electric charges and partial spin densities on the atoms demonstrated that His155 acquired positive electric charge due to the proton transfer, while the Fe(1) atom of the $[Fe_2S_2]$ cluster acquired negative charge.[14]

The geometries of the products, P2^{opt}–P6^{opt}, were optimized with the same fixed internal parameters as in M2–M6. The total energies of optimized products are presented in Table 1. For the completely optimized model M1, we could not find the product P1^{opt}, since in the course of geometry optimization the H-atom returned backward to the O atom of TMBQH. The energy of the product P2^{opt} with respect to the substrate M2 is ΔE_{opt} = = 3.6 kcal mol^{-1}. For M3–M6, the results of calculations are almost independent of the choice of the initial model. The energies of H-transfer, ΔE_{opt}, calculated as the differences between the total energies of optimized products and optimized substrates are close to zero.

The comparison of optimized structures of the substrates M2 and M3 and the products P2^{opt} and P3^{opt} showed that the quinol molecule changed its position markedly as the result of the H atom transfer. In the meantime, in the products P4^{opt}, P5^{opt}, and P6^{opt} obtained from the constrained structures M4–M6, the quinol molecule retained its position. The procedure of geometry optimization after the H-transfer mimics the structural changes in the catalytic center initiated by a rapid transfer of the atom H. In the context of the relaxation mechanism of enzyme catalysis,[15] it was interesting to evaluate the energy of the system immediately after a rapid transfer of the H atom to His155 (*i.e.*, in non-optimized system, ΔE_{nop}, see Table 1) and then to calculate the relaxation energy, $\Delta E_{rel} = \Delta E_{nop} – \Delta E_{opt}$. Here, the subscripts 'nop' and 'opt' denote the energies corresponding to non-relaxed and relaxed states of the product.

In order to get coordinates of the H atom translocated towards His155 in P^{nop}, we used two approximations. First, we placed the H atom to its position in P^{opt}. This procedure was realized by the superimposition of the structures Mi and Pi^{opt} (i = 2–6) and further deletion of the H atom from Mi and other atoms (except of the H transferred) from the Pi^{opt} structure. Second, the H atom was placed in the plane of the His155 ring, being positioned symmetrically (in the bisector of the angle C–N_ε–C) with respect to two C atoms of the ring nearby the N_ε atom. The distance $l_{H–N_\varepsilon}$ in the non-optimized products Pi^{nop} was assumed the same as in the corresponding optimized products Pi^{opt} (Table 1). The distances Δl of the H atom translocation (see Figure 1 for definition of Δl) obtained by these methods differed insignificantly (Table 1). Having evaluated the energy effects ΔE_{nop} for the H-atom transfer in the case of non-optimized products P^{nop}, we could determine the relaxation energy $\Delta E_{rel} = \Delta E_{nop} – \Delta E_{opt}$. For M4, M5, and M6, which revealed minimal RMSD values, we obtained $\Delta E_{rel} \approx 9 \pm 1$ kcal mol^{-1} (Table 1), which is close to that obtained in the previous work[8] based on the restricted Kohn–Sham method. For M2 and M3, we obtained higher values of ΔE_{rel} that can be explained by changes in the quinol position upon the geometry optimization of the product.

For M5, we also refined the structure and energy of P5^{nop} by detailed scanning of E(P5^{nop}) *versus* the position of the H atom transferred (depicted by italics in Table 1). The refined value of ΔE_{nop} appears to be the same as the minimal of approximate values. This means that for each of the models the lowest approximate value ΔE_{nop} (underlined in Table 1) should be considered as the reasonable one.

In summary, we conclude that a sufficiently large model (130 atoms) based on the crystal structure of the Cyt b_6f complex could be used for simulation of the first step of plastoquinol oxidation, provided several internal parameters (n = 18–20) were kept fixed, while other coordinates were released and could change during geometry optimization. The energy effect of the H-transfer from $TMBQH_2$ to the N_ε of His155 was estimated as ≈0 and ≈9 kcal mol^{-1} for the relaxed and non-relaxed products, respectively.

This work was supported in part by the Russian Foundation for Basic Research (grant nos. 15-04-03790a and 18-04-00214a).

Online Supplementary Materials

Supplementary data associated with this article can be found in the online version at doi: 10.1016/j.mencom.2018.03.020.

References

1 E. A. Berry, M. Guergova-Kuras, L. S. Huang and A. R. Crofts, *Annu. Rev. Biochem*., 2000, **69**, 1005.
2 J. L. Cape, M. K. Bowman and D. M. Kramer, *Trends Plant Sci*., 2006, **11**, 46.
3 A. N. Tikhonov, *Plant Physiol. Biochem*., 2014, **81**, 163.
4 D. Stroebel, Y. Choquet, J.-L. Popot and D. Picot, *Nature*, 2003, **426**, 413.
5 G. Kurisu, H. Zhang, J. L. Smith and W. A. Cramer, *Science*, 2003, **302**, 1009.
6 K.-L. Hsueh, W. M. Westler and J. L. Markley, *J. Am. Chem. Soc*., 2010, **132**, 7908.
7 M. Shimizu, N. Katsuda, T. Katsurada, M. Mitani and Y. Yoshioka, *J. Phys. Chem. B*, 2008, **112**, 15116.
8 A. E. Frolov and A. N. Tikhonov, *Russ. J. Phys. Chem. A*, 2009, **83**, 506 (*Zh. Fiz. Khim*., 2009, **83**, 593).
9 A. M. Kuznetsov, A. N. Maslii, E. M. Zueva and L. I. Krishtalik, *Zh. Fiz. Khim*., 2013, **87**, 1698 (in Russian).
10 http://molsoft.com/getbrowser.cgi?product=icm&act=list
11 L. Noodleman, T. Lovell, T. Liu, F. Himo and R. A. Torres, *Curr. Opin. Chem. Biol*., 2002, **6**, 259.
12 D. N. Laikov, *Chem. Phys. Lett*., 1997, **281**, 151.
13 J. P. Perdew, K. Burke and M. Ernzerhof, *Phys. Rev. Lett*., 1996, **77**, 3865.
14 L. Y. Ustynyuk and A. N. Tikhonov, *J. Organomet. Chem*., 2018, https://doi.org/10.1016/j.jorganchem.2018.01.023.
15 L. A. Blumenfeld and A. N. Tikhonov, *Biophysical Thermodynamics of Intracellular Processes. Molecular Machines of the Living Cell*, Springer, New York, 1994.

Received: 19th September 2017; Com. 17/5354